Third order non-linear susceptibility of InN at near band-gap wavelengths

F.B. Naranjo[a)], M. González-Herráez

Departamento de Electrónica, Escuela Politécnica, Universidad de Alcalá

Campus Universitario, 28871 Alcalá de Henares, Madrid, Spain.

H. Fernández, J. Solis

Instituto de Óptica, C.S.I.C., Serrano 121, 28006 Madrid, Spain.

E. Monroy

Equipe mixte CEA-CNRS-UJF « Nanophysique et Semiconducteurs »,

DRFMC/SP2M/PSC, CEA-Grenoble, 17 rue des Martyrs, 38054-Grenoble cedex 9,

France.

Abstract

We report room temperature measurements of the third-order non-linear susceptibility modulus, $|\chi^{(3)}|$, of thick (~600 nm) InN layers. Transmission measurements provide a room temperature value for the optical bandgap of the samples slightly above 1500 nm. Third order non-linear optical susceptibility has been measured using degenerate four wave mixing experiments at wavelengths near and above bandgap. $|\chi^{(3)}|$ values of 4.2-10 x 10^{-10} esu were measured at this wavelength range. The associated relaxation time of the generated population grating at 1500 nm was measured. The obtained value of 4.8 ps is consistent a non-radiative recombination mechanism. These figures are promising for the use of InN-based structures in all-optical devices for information processing.

a) E-mail: naranjo@depeca.uah.es

Optical third order susceptibility of materials, $\chi^{(3)}$, is the responsible of a variety of non linear phenomena, like self focusing, phase conjugation and four-wave mixing (FWM) [1]. These effects have direct applications in coherent control of optical communications. A common used technique to estimate $\chi^{(3)}$ modulus is by performing forward degenerate four wave mixing (DFWM) measurements [2]. The physical principle underlying FWM has been employed, for instance, to control the speed of light in GaAs quantum structures at 850 nm using the so-called population oscillation (PO) effect [3,4]. Thus, materials with large third order nonlinear susceptibility are required for fabrication of all optically-controlled devices, like all-optical switches and wavelength converters [5].

Semiconductor band-gap engineering allows the development of compact and transportable devices, with tuneable operation wavelength. InN is particularly attractive for telecommunications, due to its room-temperature band-gap around 1500-1600 nm [6]. In the last years, progress in InN deposition techniques has made possible to improve its structural quality, and has lead to a redefinition of many structural and optical properties of this material.

In this work we have determined the third order susceptibility, $|\chi^{(3)}|$ of InN films grown by plasma-assisted molecular-beam epitaxy (PAMBE) by using DFWM with excitation at energies around and above the bandgap (1500 and 1400 nm). The same technique has been used to determine the relaxation time of the excited carrier populations [7].

In-face polarity InN samples were grown by PAMBE in a chamber equipped with standard effusion cells for In and Ga, and a radio-frequency plasma cell to supply active nitrogen. Substrates consisted of 10-µm-thick non-intentionally doped (n.i.d.) GaN-on-sapphire templates. Prior to the growth of the InN layer, a 10-nm-thick n.i.d.

GaN buffer layer was deposited at 720ºC. InN growth was carried out at a substrate temperature of 450°C, with a N flux corresponding to a growth rate of 0.3 monolayers per second, and with an In/N ratio of 1.2. This high III/V ratio is required to achieve two-dimensional growth. Since the desorption rate of In is lower than the decomposition rate of InN [8], it is not possible to stabilize an autoregulated layer of In on the InN surface, as we demonstrated on GaN [9]. Therefore, periodic growth interruptions under N are performed to consume the In excess and prevent the accumulation of In droplets on the surface. The growth period (InN growth time / growth interruption time) of the samples and their total growth time are summarized in Table I. Taking into account the excess of In accumulated on the InN surface during growth, samples E1 and E2 are considered to be grown under slightly In-rich and N-rich conditions, respectively.

The structural quality of the samples was assessed by high-resolution x-ray diffraction (HRXRD) and atomic force microscopy (AFM). The full width at half maximum (FWHM) of the ω-scan of the (0002) refection of the InN layers, and the rms roughness measured in a surface of 5×5 μm^2 are summarized in Table I. In the case of E1, we observe a reasonable rocking curve of 640 arcsec and a surface roughness of 0.81 nm, comparable to standard values achieved for Ga-face GaN. In the case of E2, were the accumulation time of In is lower, there is a clear degradation of the structural quality.

Linear optical properties of the samples in the wavelength range of 1100-2550 nm were studied by room-temperature transmission measurements at normal incidence using a Perking-Elmer scanning spectrophotometer. Experimental results were compared with theoretical transmittance spectra generated using a three layer model (sapphire/GaN/InN) [11], to obtain values of thickness, ordinary refractive index, $n_0(\lambda)$, and absorption coefficient, $\alpha(\lambda)$, of the InN layer. First order Sellmeier dispersion

formulae were considered for index refraction in the transparency region [12]. Besides, a sigmoidal approximation was used for $\alpha(\lambda)$ for sample E1 [13], while a deep level defect with |s> like symmetry was taken into account for sample E2 [14]. Transmission data of GaN substrate was analyzed considering a two layer structure (sapphire/GaN). An index refraction of 2.23 was estimated for the 1400-1500 nm wavelength range, where the absorption was considered negligible.

Figures 1(a) and (b) show calculated and measured transmission data, together with the absorption coefficient for samples E1 and E2, respectively. The room temperature absorption band edge is estimated at 1550 nm and 1510 nm for samples E1 and E2 respectively. From these values we can conclude that the samples are suitable for third order optical non-linear susceptibility measurements around 1500 nm. Table II summarizes the linear optical estimations performed for 1400 and 1500 nm applied to the subsequent $|\chi^{(3)}|$ calculation.

Following the results obtained for linear optical properties of the samples, non-linear measurements were carried out. The optical non-linear characterization was performed by the DFWM technique in the forward configuration (BOXCARS) [2] using as excitation source an optical parametric amplifier (OPA) providing 100 fs pulses, tuneable in the 300-3000 nm interval, at a repetition rate of 1KHz. In the DFWM measurements the conjugated beam intensity, I_C, is plotted versus the pump intensity, I_P, to obtain the coefficient c of the relationship $I_C = cI_P^3$. The third order susceptibility of the samples, $|\chi_S^{(3)}|$ is then obtained using eq. (1), which relates the non-linear susceptibility of a given sample and that of a reference material with their corresponding optical parameters and conjugated signals:

$$\left|\chi_s^{(3)}\right| = \left(\frac{n_0^s}{n_0^r}\right)^2 \left(\frac{L^r}{L^s}\right) \left(\frac{c^s}{c^r}\right)^{1/2} \frac{\alpha L^s e^{\alpha L/2}}{1-e^{-\alpha L}} \left|\chi_r^{(3)}\right| \qquad (1)$$

where n_0, L and α are the ordinary linear refractive index, the interaction length and absorption coefficient respectively, while superscripts r and s indicate parameters concerning the reference and the sample. A fused silica plate ($|\chi_r^{(3)}|$ = 1.28x 10^{-14} esu and n_0=1.45, [2]) was used as reference sample for the measurements.

In the experiment, a linear noise background caused by scattering at the sample is spatially overlapped to the conjugated beam. Considering the very small interaction lengths involved in the experiment (a few hundreds of nm), this background signal can be extremely detrimental for performing a precise determination of $|\chi_s^{(3)}|$. Accordingly, this background was minimized by spatial filtering the conjugated beam before measuring its intensity using an InGaAs photodiode. Additionally, the remnant linear noise background was measured for different pump beam powers by introducing a large negative delay (~100 ps) between one of the pumps and the others thus cancelling the non-linear interaction. The so-determined signal was then subtracted for each pump power from the experimentally measured conjugated signal value. Under these conditions, when the conjugated beam is present, the relationship between its intensity and pump beams intensity is necessarily cubic [2]. Additional details about the DFWM setup can be found in Ref. [10].

The third order susceptibility of the GaN substrate was measured for 1400 nm and 1500 nm wavelengths to obtain its possible contribution to the measurements performed in the InN films. In this case, no DFWM signal was detected for pump beam intensities below 3.5 GW/cm^2. Above this pump intensity, a value of 4.4±0.4 x 10^{-12} esu was obtained for the considered wavelengths. This result is in the order of the values obtained theoretically by Nayak et al, of 0.16 x 10^{-12} esu for zinc-blende GaN structure [15] and by Sun et al. of 0.7 x 10^{-12} at 1230 nm, using third harmonic generation [16].

The InN samples were thus measured with a pump beam intensity below the above indicated value to ensure a negligible contribution from the GaN substrate. Figure 2 shows a representative plot of I_C versus I_P for the GaN substrate and the E1 film, showing the negligible contribution of the substrate to the film signal. Table II summarizes the measured values of $|\chi^{(3)}|$. Considering the above described procedure for minimizing the spurious contribution of scattering to the measured conjugated signal, is clear that the apparently poor cubic fitting obtained is simply related to the relatively low value of $|\chi^{(3)}|$ obtained and to the very small thickness of the analyzed layers (only 600 nm). The value of the error bars included in the plot are related to this as well as to the fluctuations of the pump beam energy (~6%).

The close to resonant character of $|\chi^{(3)}|$ for InN in the range of wavelengths studied leads to values two order of magnitude higher than the ones obtained for GaN. For E1, $|\chi^{(3)}|$ increases with α, due to the close-to-resonant wavelength range. The measured values differ from theoretical predictions by Nayak *et al.* [15] of 10^{-12} esu, calculated for the previously assumed InN bandgap of 1.9 eV. E2 shows a lower value of $|\chi^{(3)}|$ when compared to sample E1 despite its higher optical density, αL (1500 nm and 1400 nm, respectively). This fact could be explained in terms of the Bursten-Moss shift of the material optical bandgap observed in the linear absorption measurements (see figure 1). Obtained values of $|\chi^{(3)}|$ for InN are comparable to the value of semiconductors commonly used for communication applications, like InGaAsP, with estimated $|\chi^{(3)}|$ of 4.2 x 10^{-10} esu [17]. Nevertheless, its application in the development of all-optical processing devices would probably require the use of InN-based structures with lower dimensionality, to increase the resultant $|\chi^{(3)}|$ value [18].

We have determined the lifetime, τ_G, of the conjugated signal (associated to the dynamic grating induced at 1500 nm) for sample E1 by varying the delay between one

of the pumps and the others using an optical delay line. Inset of figure 2 shows the conjugated-signal intensity as a function of the induced delay time, showing an exponential decay [7]. The lifetime estimated from this exponential decay is of 4.8 ps at room temperature, comparable to the value of 12 ps, obtained by Hu *et al.* in a AsGa quantum dot based semiconductor optical amplifier, used to obtain room temperature *slow* and *fast* light [19]. This lifetime, related to a carrier concentration grating or phase grating, is given by the equation [7]:

$$\frac{1}{\tau_G} = \frac{1}{\tau} + \frac{4\pi^2 D}{\Lambda^2} \tag{2}$$

,where τ is the carrier recombination time (τ_R), and the dephasing time (τ_D) for the carrier concentration and the phase grating, respectively. Second term of eq. 2 accounts for the diffusion of the carriers, where D is the diffusion coefficient and Λ is the grating fringe spacing, given by $\lambda / 2\sin(\theta/2)$, being θ the angle between pump beams. Within the experimental conditions of this work, measured τ_G would lead to D~7800 cm^2/s, three orders of magnitude higher than typical values [20] allowing to discard diffusion as the origin of the observed lifetime. Radiative carrier lifetime can be estimated through the expression $[B_r(n_0 + \Delta n)]^{-1}$, with B_r, the bimolecular radiative recombination coefficient ~0.3×10^{-10} $cm^3 s^{-1}$ [21], n_0~1×10^{19} the free carrier concentration of the samples, and Δn ~1×10^{19} cm^{-3} the photoexcited carrier concentration, leading to a value of ~2 ns, much longer than the experimentally determined one. On the other hand, dephasing time measurements on GaN leads to values of just 150 fs [22]. Thus τ_G can be attributed to a non-radiative carrier relaxation mechanism in good agreement with the 16 ps value obtained by H. Haag *et al.* for GaN in DFWM experiments [23]. Carrier recombination could take place at the defects responsible for the free carrier concentration of the samples. The origin of measured $\chi^{(3)}$

is thus the excitation-dependent change in refractive index and absorption coefficient of the material associated to the dynamical modification of the carrier concentration caused by a near band edge excitation. Any possible cumulative thermal effects in the experiment can be neglected by considering the low laser repetition rate used (1 kHz).

In summary, third order optical non linear susceptibility of InN layers grown by PAMBE has been measured using DFWM. Third-order non-linear susceptibility modulus, $|\chi^{(3)}|$, values of 4.2-10 x 10^{-10} esu were measured at wavelength ranges from 1400 nm to 1500 nm. Relaxation time of the generated population grating was estimated to be 4.8 ps at 1500 nm, being attributed to non-radiative carrier recombination.

Thanks are due to Prof. P. Corredera and Dr. S. Fernández for valuable suggestions. Partial financial support was provided by Spanish government projects TEC2006-09990-C02-02/TCM and TEC2005-00074/MIC, and by Comunidad de Madrid, Project S-0505/AMB-0374.

References

[1] A. Miller, D.A. B. Miller, and S. D. Smith, Advances in Phys. **30**, 697 (1981).

[2] R.L. Sutherland, "Handbook of nonlinear optics" Marcel Dekker, Inc., New York, 1996.

[3] Shu-W. Chang, Shun-L. Chuang, Pei-C. Ku, C.J. Chang-Hasnain, P. Palinginis, and H. Wang, Physical Review B 70, 235333 (2004).

[4] P. Palinginis, F. Sedgwick, S. Crankshaw, M. Moewe, and C.J. Chang-Hasnain, Optics Express **13**, 9909 (2005).

[5] D. Cotter, R. J. Manning, K. J. Blow, A. D. Ellis, A. E. Kelly, D. Nesset, I. D. Phillips, A. J. Poustie, and D. C. Rogers, Science 286 1523 (1999).

[6] K. S. A. Butcher, and T.L. Lansley, Superlattices and Microstructures **38**, 1 (2005).

[7] S. Adachi, Y. Takagi, J. Takeda, and K.A. Nelson, Optics Communications **174**, 291 (2000).

[8] C. S. Gallinat, G. Koblmüller, J. S. Brown, S. Bernardis, J. S. Speck, G. D. Chern, E D. Readinger, H. Shen, and M. Wraback, Appl. Phys. Lett. **89**, 032109 (2006).

[9] E. Monroy, B. Daudin, E. Bellet-Amalric, N. Gogneau, D. Jalabert, F. Enjalbert, J. Brault, J. Barjon, and Le Si Dang, J. Appl. Phys. **93**, 1550 (2003).

[10]. R. del Coso, J. Requejo-Isidro, J. Solis, J.Gonzalo, and C. N. Afonso, J.Appl.Phys. **95**, 2755 (2004)

[11] M.J. Bergman, Ü. Özgür, H.C. Casey, J.F. Muth, Y.C. Chang, R.M. Kolbas, R.A. Rao, C.B Eom, and M. Schurman, Appl. Phys. Lett. **74**, 3188 (1999).

[12] N. Antoine-Vincent, F. Natali, M. Mihailovic, A. Vasson, J. Leymarie, P. Disseix, D. Byrne, F. Semond, and J. Massies, J. Appl. Phys. **93**, 5222 (2003).

[13] F.B. Naranjo, M.A. Sánchez-García, F. Calle, E. Calleja, B. Jenichen, and K.H. Ploog, Appl. Phys. Lett. **80**, 231 (2002).

[14] K.S.A. Butcher, M. Wintrebert-Fouquet, P.P.-T. Chen, H. Timmers, and S.K. Shrestha, Mat. Sci. in semicond. Processing **6**, 351 (2003).

[15] S.K. Nayak, T. Sahu, S.P. Mohanty, and P.K. Misra, Semicond. Sci. Technol. **12**, 544 (1997).

[16] C.-K. Sun, S.-W. Chu, S.-P. Tai, S. Keller, U. K. Mishra, and S. P. DenBaars, Appl. Phys. Lett. **77**, 2331 (2000).

[17] J.P. Donnelly, H.Q. Le, A. Swanson, S.H. Groves, A. Darwish, and E.P. Ippen, IEEE Phot. Technol. Lett. 8, 623 (1981).

[18] K.D. Choquette, L. McCaughan, and D.K. Misemer, J. Appl. Phys. **66**, 4387 (1989).

[19] H. Su, and S.L. Chuang, Appl. Phys. Lett. **88**, 061102 (2006).

[20] A.G. Bhuiyan, A. Hashimoto, and A. Yamamoto, J. Appl. Phys. **94**, 2779 (2003).

[21] U. Strauss, W. W. Ruhle, H. J. Queisser, K. Nakano, and A. Ishibahi, J. Appl. Phys. **75**, 8204 (1994).

[22] K.-H. Lin, G.-W. Chern, Y.-C. Huang, S. Keller, S.P. DenBaars, and C.-K. Sun, Appl. Phys. Lett. **83**, 3087 (2003).

[23] H. Haag, S. Petit, P. Gilliot, R. Lévy, O. Briot, and R.L. Aulombard, Mater. Sci. Engineer. **B50**, 197 (1997).

Table I: Growth conditions and structural characterization of the samples under study.

Sample	Growth sequence (InN grown / N exposure)	Total growth time	FWHM ω (0002)	rms roughness
E1	5 min / 1 min	130 min	640 arcsec	0.81 nm
E2	30 s / 6 s	100 min	1260 arcsec	2.9 nm

Table I. F.B. Naranjo *et al.*

Table II. Summary of results obtained from linear and non-linear optical measurements. For sample E2, poor signal-to-noise ratio hinders reliable measurements at 1500 nm.

Sample	Thickness (nm)	Wavelength (nm)	α (cm^{-1})	n	αL	$\lvert\chi^{(3)}\rvert$ (esu)
E1	650	1400 nm	1.4×10^{4}	2.95	0.90	$1.0 \pm 0.1 \times 10^{-9}$
		1500 nm	4.7×10^{3}	2.86	0.30	$5.4 \pm 0.6 \times 10^{-10}$
E2	680	1400 nm	8.7×10^{3}	2.78	0.60	$4.2 \pm 0.4 \times 10^{-10}$
		1500 nm	3.1×10^{3}	2.77	0.21	-

Table II. F.B. Naranjo *et al.*

Figure captions.

Figure 1. Experimental and calculated room-temperature transmission spectra, together with the calculated absorption coefficient, for samples (a) E1 and (b) E2

Figure 2. I_s-I_p plot for GaN template and sample E1 at 1400 nm, showing the negligible effect of the substrate. Inset shows DFWM signal intensity obtained for sample E1 at 1500 nm as a function of delay time between one of the pumps and the others. The exponential decay fit used to calculate the conjugated-signal lifetime is also shown (full line).

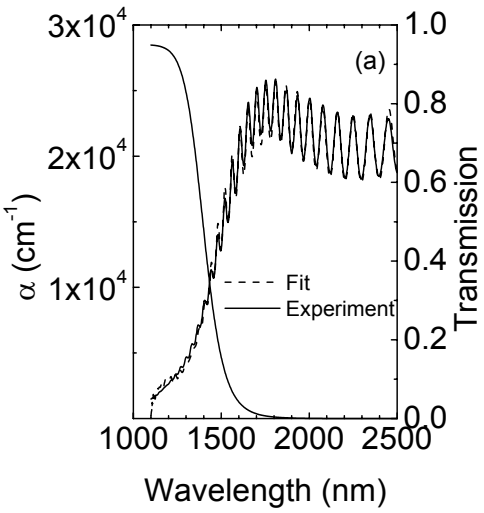
(a)
3x10^4
2x10^4
1x10^4
α (cm^-1)
1.0
0.8
0.6
0.4
0.2
0.0
Transmission
Fit
Experiment
1000 1500 2000 2500
Wavelength (nm)

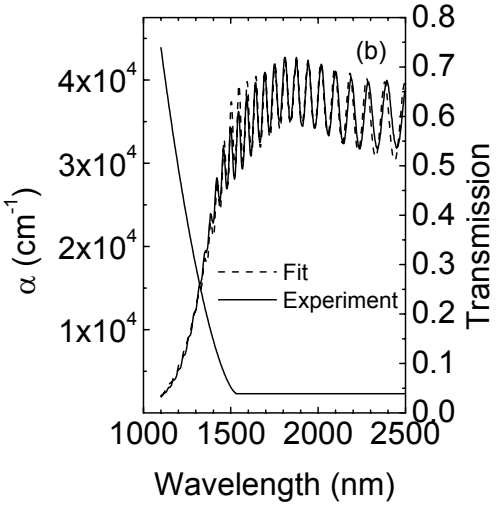
(b)
4x10^4
3x10^4
2x10^4
1x10^4
α (cm^-1)
0.8
0.7
0.6
0.5
0.4
0.3
0.2
0.1
0.0
Transmission
Fit
Experiment
1000 1500 2000 2500
Wavelength (nm)

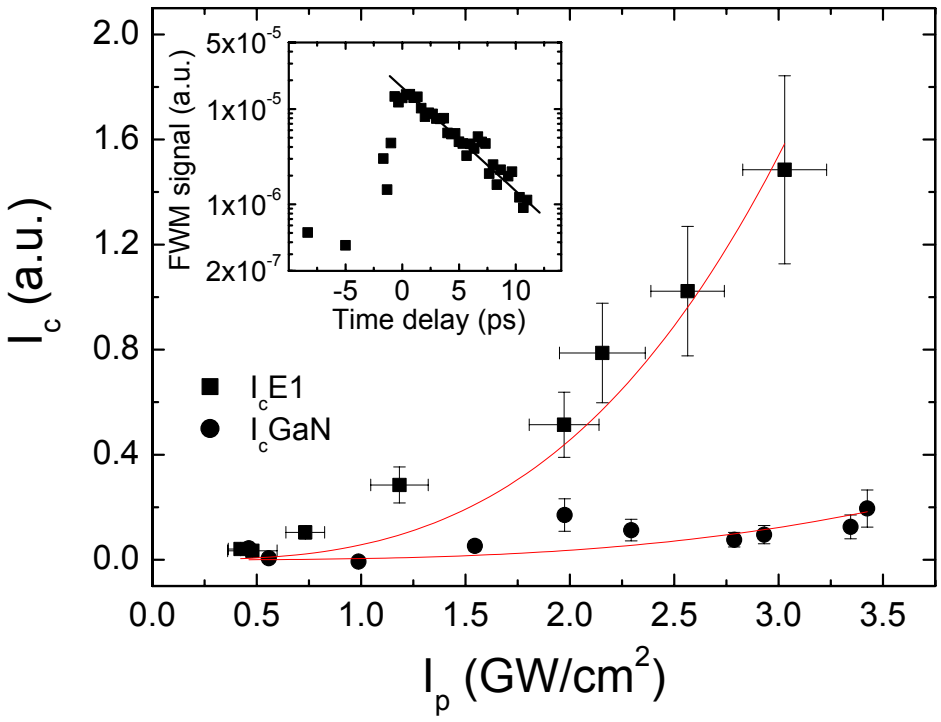
2.0
1.6
1.2
0.8
0.4
0.0
I_c (a.u.)
0.0
0.5
1.0
1.5
2.0
2.5
3.0
3.5
I_p (GW/cm^2)
I_cE1
I_cGaN
5x10^{-5}
1x10^{-5}
1x10^{-6}
2x10^{-7}
FWM signal (a.u.)
-5
0
5
10
Time delay (ps)